Journal of
Mechanics of
Materials and Structures

CONICAL INDENTATION OF THICK ELASTIC SPHERICAL SHELLS

Nkem Ogbonna and Alan Needleman

CONICAL INDENTATION OF THICK ELASTIC SPHERICAL SHELLS

NKEM OGBONNA AND ALAN NEEDLEMAN

Indentation of spherical shells by a rigid conical indenter is analyzed. Because the shape change associated with overall bending provides a main deviation from the corresponding indentation behavior of a half-space, finite deformation analyses are carried out. The shell material is characterized by a hypoelastic relation that reduces to isotropic linear elasticity for small strains and is an elastic relation at finite strains for fixed principal directions. Axisymmetric deformations are assumed. For indentation of shells there is a complex interaction between the indentation response and the overall structural response of the shell. The aim of the analyses is to give insight into the range of indentation depths for which the indentation response dominates so that an indentation analysis can be used to extract the elastic properties. Shells having various thicknesses are analyzed. It is found that for spherical shells with thickness to radius ratios less than or equal to 0.4 and for sufficiently shallow indentation depths, the scaling of the indentation load with contact area has the same form as that for indentation into a half-space but with a different scaling constant.

1. Introduction

Indentation is a convenient method for investigating the mechanical properties of solids that are difficult to characterize by other mechanical testing methods. It is relatively nondestructive and is routinely used to measure the elastic stiffness and hardness of a wide variety of solids at a variety of scales; see, for example, [Doerner and Nix 1986; Oliver and Pharr 1992; Oliver and Pharr 2004]. Indentation has also been explored for determining the yield strength and strain hardening index of thin films [Cheng and Cheng 1998; Ma et al. 1998].

An indentation test is typically performed on a flat surface of a solid. An indenter of prescribed geometry is pressed into the solid under prescribed load and the depth of penetration and/or the size of the contact are measured. For depth-sensing indentation tests, the mechanical properties are determined directly from load and displacement measurement. Various indenter profiles are used: the most common ones include a cone (Rockwell test), a sphere (Brinell test), a rectangular pyramid (Vickers test) and a triangular pyramid (Berkovich test).

Much is known about indentation of solids, particularly elastic and elastic-plastic solids [Johnson 1985; Barber and Ciavarella 2000]. For indentation of a conical indenter into an isotropic linear elastic solid that can be appropriately idealized as being a half space, there is no characteristic dimension other than the indentation depth. Hence, from dimensional considerations,

$$\frac{P}{Eh^2} = K,$$

Keywords: indentation, elasticity, spherical shells, finite element modeling.

where P is the indentation force, E is Young's modulus, h is the indentation depth and K is a constant. The value of K depends on the shape of the cone cross section, the cone angle and Poisson's ratio, and can be determined from the solution of an elasticity problem. With K known, measuring the indentation force and depth enables E to be directly determined. A recent comprehensive overview of indentation into a planar linear elastic solid has been given in [Poon et al. 2008]. Much of the interest in indentation of linear elastic solids has been associated with characterizing the unloading response of elastic-plastic solids that have been indented [Oliver and Pharr 2004].

Some solids, such as natural and biological materials, may not have flat surfaces available for indentation. For example, the outer surface of the human eye is dome-shaped and, in order to determine intraocular pressure, doctors usually subject it to an indentation test using an instrument called a tonometer. The growing interest in natural materials, which often involve shell-type structures, as potential renewable resources for high performance and cost effective structural applications provides another motivation for examining the indentation behavior of solids with curved surfaces.

There is a literature on the deformation of thin elastic shells subject to point type loads that can give rise to complex deformation patterns; see for example [Vaziri and Mahadevan 2008]. However, the focus here is on relatively thick shells for which the deformation pattern remains axisymmetric when subject to conical indentation. We also neglect any effect of adhesion which can play an important role in contact of elastic solids as shown in [Johnson et al. 1971]. In this paper, we explore the extent to which simple scaling relations can be used to extract elastic moduli of isotropic elastic solids from indentation of spherical shells by a rigid conical indenter. In particular, we consider indentation of a rigid conical indenter with a circular cross-section into a thick walled isotropic linear elastic spherical shell. Indentation of a cone into a solid sphere has been considered in [Fu 2007]. A fundamental difference between indentation of a cone into a half space and its indentation into a spherical shell is that for the shell geometry there are characteristic lengths other than the indentation depth h. For a spherical shell with internal radius R_i and external radius R_o,

$$\frac{P}{Eh^2} = C\left(\frac{h}{R_i}, \frac{R_i}{R_o}\right),$$

so that extracting the value of Young's modulus E from a measurement of indentation force and depth is not necessarily as straightforward as for a half space. Although our interest is in linear elastic material response, we carry out finite deformation analyses because for shells a main deviation from linearity is associated with a change in shape due to bending.

2. Problem formulation

The problem we analyze is indentation of a linear elastic spherical shell by a rigid conical indenter allowing for the possibility of finite shape changes. The finite element implementation is based on a convected coordinate Lagrangian formulation of the field equations, with the initial unstressed state taken as reference. All field quantities are taken to be functions of convected coordinates, y^i, which serve as particle labels, and time, t. With attention confined to quasi-static deformations and with body

forces neglected, the rate form of the principal of virtual work is

$$\int_V [\dot{\tau}^{ij}\delta E_{ij} + \tau^{ij}\dot{u}^k_{,i}\delta u_{k,j}]\,dV = \int_S \dot{T}^i \delta u_i \, dS. \tag{2-1}$$

Here, V and S are the volume and surface, respectively, of the body in the reference configuration and $(\dot{\ }) = \partial()/\partial t$ at fixed y^i. The contravariant components of the Kirchhoff stress, τ^{ij}, are given by $\tau^{ij} = J\sigma^{ij}$, where J is the ratio of current to reference volume of a material element and σ^{ij} are the contravariant components of the Cauchy (or true) stress on the deformed convected coordinate net.

The nominal traction components, T^i, and the Lagrangian strain components, E_{ij}, are given by

$$T^i = (\tau^{ij} + \tau^{kj}u^i_{,k})\nu_j, \tag{2-2}$$

$$E_{ij} = \tfrac{1}{2}(u_{i,j} + u_{j,i} + u^k_{,i}u_{k,j}), \tag{2-3}$$

where u_j are the components of the displacement vector on base vectors in the reference configuration, $(\ )_{,i}$ denotes covariant differentiation in the reference frame and ν_j are the surface normal components in the reference configuration.

The material is described by a constitutive relation of the form

$$\hat{\tau}^{ij} = L^{ijkl}\dot{E}_{kl}, \tag{2-4}$$

where $\hat{\tau}^{ij}$ is the Jaumann derivative of the Kirchhoff stress and

$$L^{ijkl} = \frac{E}{1+\nu}\left[\frac{1}{2}\left(G^{ik}G^{jl} + G^{il}G^{jk}\right) + \frac{1}{1-2\nu}G^{ij}G^{kl}\right], \tag{2-5}$$

with G^{ij} being the contravariant components of the metric tensor in the current configuration. The relation in (2-4) and (2-5) is a hypoelastic relation but does reduce to isotropic linear elasticity for small strains and is an elastic relation at finite strains for fixed principal directions.

Figure 1 is a sketch of the indenter and the definition of the angle β. The contact radius a is defined as the actual contact radius accounting for sink in. The corresponding indentation depth h is then defined by

$$h = a\tan\beta \tag{2-6}$$

The spherical shell has internal radius R_i and external radius R_o so that the shell thickness is $t = R_o - R_i$. Axisymmetric deformations are assumed. Figure 2 shows the region analyzed and finite element mesh used for a shell with $t/R_o = 0.4$.
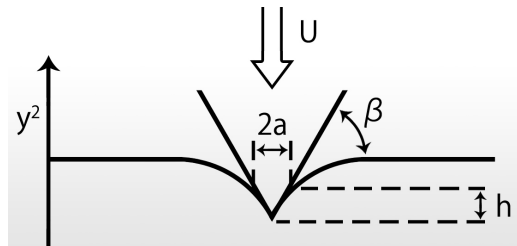

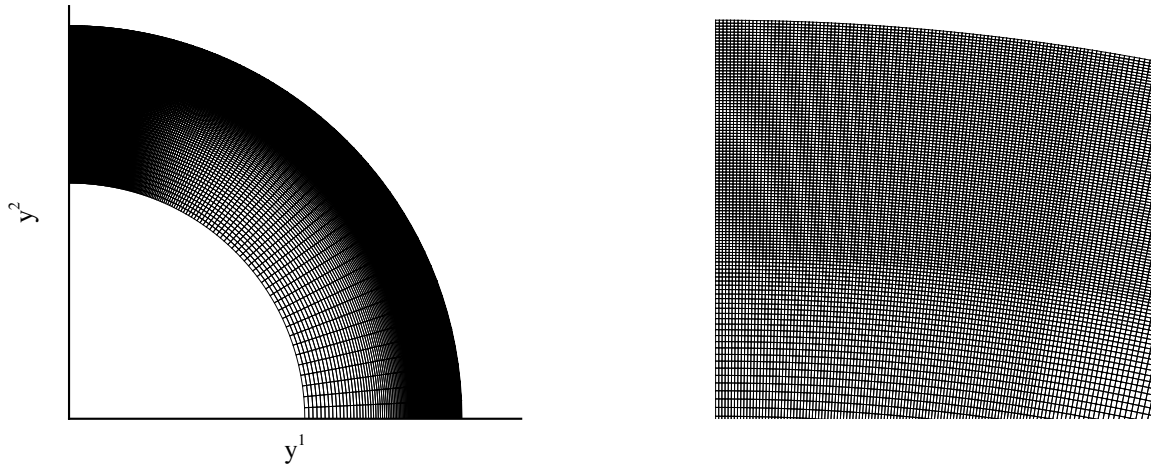**Figure 1.** A sketch of the indenter geometry.

Figure 2. The finite element mesh for a spherical shell with $t/R_o = 0.4$. Each quadrilateral consists of four "crossed" triangular linear displacement elements. Left: the full mesh. Right: the fine mesh region.

Perfect sticking is assumed as soon as the shell comes into contact with the indenter, so that the rate boundary conditions are

$$\dot{u}_1 = 0 \qquad \dot{u}_2 = -\dot{U} \qquad \text{on} \quad S_{\text{contact}}, \tag{2-7}$$

where S_{contact} denotes the portion of the shell surface in contact with the indenter and U is the imposed displacement of the rigid indenter. Note that U is not equal to h as defined here where h is the depth associated with the contact radius. Initially, S_{contact} is the single point $y^1 = 0$, $y^2 = R_o$. As additional points come into contact, S_{contact} expands.

The symmetry conditions on the y^2–axis are

$$\dot{u}_1 = 0 \qquad \dot{T}^2 = 0 \quad \text{on} \quad y^1 = 0. \tag{2-8}$$

Symmetry is also assumed about the y^1–axis so that

$$\dot{u}_2 = 0 \qquad \dot{T}^1 = 0 \quad \text{on} \quad y^2 = 0, \tag{2-9}$$

and the remaining external surfaces are traction free so that $\dot{T}^1 = \dot{T}^2 = 0$.

The finite element discretization of (2-1) is based on linear displacement triangles arranged into "crossed" triangle quadrilaterals and the deformation history is calculated in an incremental manner. Calculations are carried out for four values of the thickness to radius ratio, t/R_o, 0.1, 0.2, 0.4 and 0.6. Different finite element meshes are used for each value of t/R_o. For $t/R_o = 0.6$, a 155×220 quadrilateral mesh is used with a uniform 100×100 quadrilateral mesh in a region $t/R_o = 0.1 \times \Delta\theta = 9°$ near the indenter. Here, $R = \sqrt{(y^1)^2 + (y^2)^2}$ and $\theta = \tan^{-1}(y^2/y^1)$. This mesh has 34100 quadrilaterals and 68592 degrees of freedom after static condensation is used to eliminate the central node in each quadrilateral. The mesh for $t/R_o = 0.4$, shown in Figure 2, has 140×220 quadrilaterals, giving 62322

degrees of freedom after static condensation and the uniform mesh is 80×100 in a $t/R_o = 0.1 \times \Delta\theta = 9°$ region near the indenter. The corresponding values for $t/R_o = 0.2$ are 100×220, 44642 and an 80×100 uniform mesh in a $t/R_o = 0.1 \times \Delta\theta = 9°$ uniform region and for $t/R_o = 0.1$, 100×200, 40602 and an 90×100 uniform mesh in a $t/R_o = 0.15 \times \Delta\theta = 9°$ uniform region.

3. Results

For indentation of a rigid conical indenter into a flat surface we have (see [Sneddon 1948; Johnson 1985])

$$\frac{P}{Ea^2} = \frac{\pi}{2} \frac{1}{(1 - \nu^2)} \tan\beta. \tag{3-1}$$

Alternatively, expressed in terms of the contact depth $h = a \tan\beta$,

$$\frac{P}{Eh^2} = \frac{\pi}{2} \frac{1}{(1 - \nu^2)} \frac{1}{\tan\beta} = \frac{\pi}{2} \frac{1}{(1 - \nu^2)} \cot\beta. \tag{3-2}$$

The relation (3-2) is sometimes expressed in terms of the displacement of the rigid indenter, here termed U, for example in [Poon et al. 2008]. For indentation of a rigid cone into a linear elastic half-space $h = (2/\pi)U$; see [Bower et al. 1993], for example.

With $\beta = 20°$, (3-2) gives $P/(Eh^2) = 4.74$. A finite element calculation using the formulation in Section 2 but for indentation into a flat surface gave $P/(Eh^2) = 4.90$.

For spherical shells, calculations were carried out for $t/R_o = 0.1, 0.2, 0.4, 0.6$. In all calculations, Poisson's ratio ν, was taken to be 0.3 and, unless otherwise stated, the indenter angle β is fixed at $20°$. The calculations were carried out for prescribed increasing displacement U.

The relation between h and U for the spherical shells analyzed is shown in Figure 3. For U/R_o sufficiently small, the half-space relation provides an accurate characterization and for $h/R_o = 0.4$ and
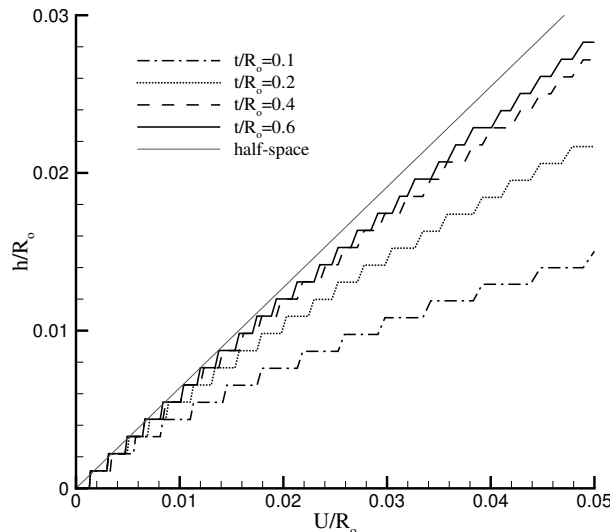

Figure 3. Variation of the indentation depth h associated with the current contact radius a versus the displacement of the rigid indenter U.
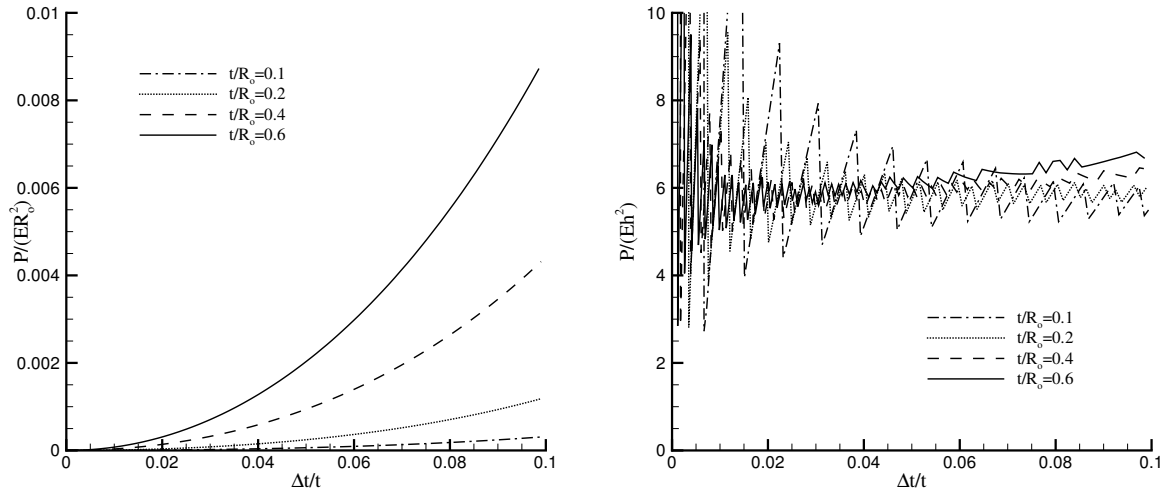
Figure 4. Variation of normalized contact force P/ER_o^2 (left) and normalized contact pressure P/Eh^2 with the change in shell thickness under the indenter (i.e., at $y^1 = 0$) for spherical shells with $t/R_o = 0.1, 0.2, 0.4, 0.6$.

0.6 that relation is approximately satisfied up about $U/R_o = 0.02$. For U/R_o greater than about 0.02 there are significant deviations with the deviation increasing with decreasing shell thickness.

Curves of contact force normalized by Young's modulus E and the outer sphere radius R_o, P/ER_o^2, plotted against $\Delta t/t$, are shown in Figure 4. The quantity $\Delta t/t$ is the change in thickness divided by the original thickness of the shell at $y^1 = 0$ and is convenient for representing the indentation depth. There is a clear dependence of the indentation force on the shell thickness, with the thinner shells requiring a smaller contact force for a given indentation depth. The indentation force at a given value of $\Delta t/t$ does not quite scale with t^2; for example, at $\Delta t/t = 0.08$, the indentation force with $t/R_o = 0.6$ is 7.8 times that for $t/R_o = 0.2$ and 30.4 times that for $t/R_o = 0.1$.

However, when the contact depth $h = a \tan \beta$ is used to normalize the indentation force there is a range where the value of P/Eh^2 is nearly the same for all four values of the shell thickness. The oscillations are a numerical artifact due to the contact radius increasing by an element length when a new node comes into contact with the indenter whereas the contact force increases smoothly. When only a few nodes are in contact with the indenter, the contact area is too small for an accurate value of P/Eh^2 to be obtained. A finer finite element mesh would permit accurate values of P/Eh^2 to be obtained for smaller indentation depths $\Delta t/t$. At larger values of indentation depth, a reasonably accurate estimate of P/Eh^2 can be obtained. For example, $\Delta t/t = 0.035$, the value of P/Eh^2 lies between 5.9 and 6.1 for all four values of t/R_o. The mean value of P/Eh^2 for $t/R_o = 0.1$ and 0.2 is 5.9. The mean values of P/Eh^2 are a bit higher and, furthermore, clearly increase with increasing indentation depth for $\Delta t/t$ greater than about 0.05. The value of normalized contact force, P/Eh^2, for the spherical shells is significantly greater than for indentation into a flat surface for the same material and the same indenter angle, ≈ 6 versus the numerically obtained value of 4.9 for indentation of a flat surface.

The dependence of the indentation pressure on the angle β is shown in Figure 5 for a spherical shell having $t/R_o = 0.4$. The evolution of the normalized contact force P/Eh^2 is plotted against the contact
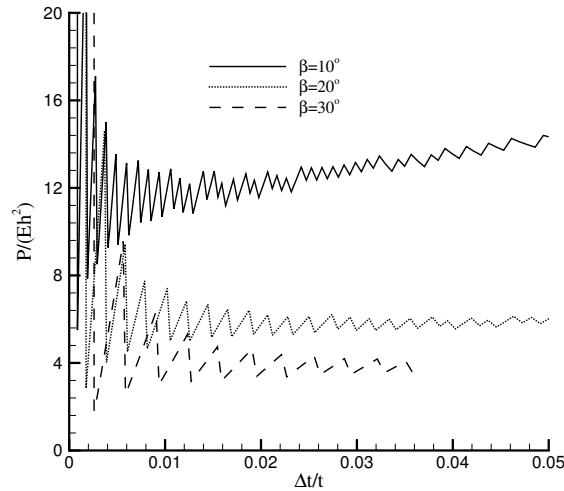
Figure 5. Variation of normalized contact pressure, P/Eh^2, with indenter angle β for spherical shells with $t/R_o = 0.4$.

depth as measured by $\Delta t/t$. For $\beta = 30°$, the mean value of P/Eh^2 is 3.8, for $\beta = 20°$ it is 5.9 and for $\beta = 10°$ it is about 12. For the most flat cone geometry, $\beta = 10°$, the mean value of P/Eh^2 increases with $\Delta t/t$ over the entire range for which a reliable estimate of P/Eh^2 can be obtained. This is not surprising since in the limit of a flat surface pressing against a spherical shell, the deformation is dominated by overall shell bending. Nevertheless, for all three values of β, the dependence of P/Eh^2 on $\tan\beta$ follows the scaling in (3-2). The ratio $\cot 30°/\cot 20°$ equals 0.631, while the corresponding ratio of normalized contact force in Figure 5 is 0.644. Even for $\beta = 10°$ we have $\cot 10°/\cot 20° = 2.06$, while $12/5.9 = 2.03$.

Distributions of mean normal stress $\tau_k^k/3$, where $\tau_k^k = G_{km}\tau^{km}$, normalized by Young's modulus E, are shown in Figure 6 for $t/R_o = 0.6$ and 0.2. These plots also show the deformed shape of the spherical shells at $\Delta_t/t = 0.1$. The mean normal stress is negative and a significant fraction of Young's modulus
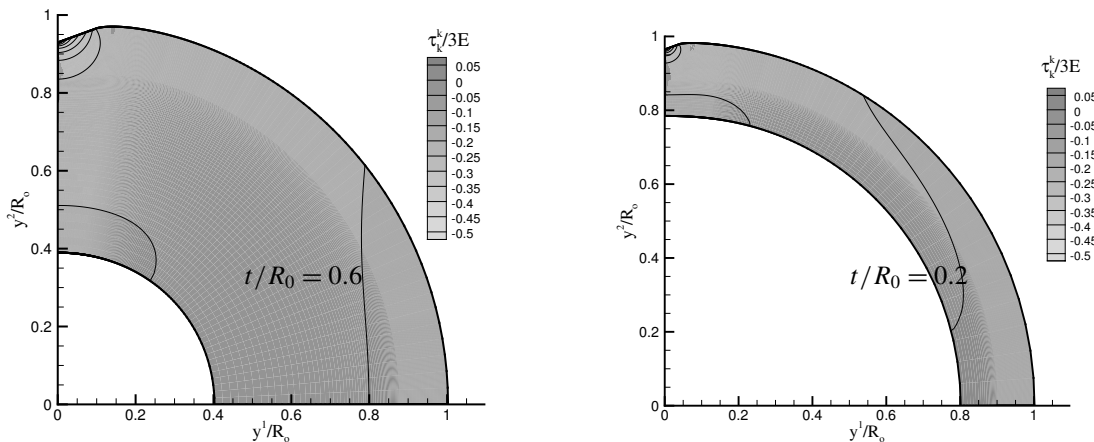

Figure 6. Contours of $\tau_k^k/3E$ at $\Delta t/t = 0.1$ for shells with $t/R_o = 0.6$ and $t/R_o = 0.2$.
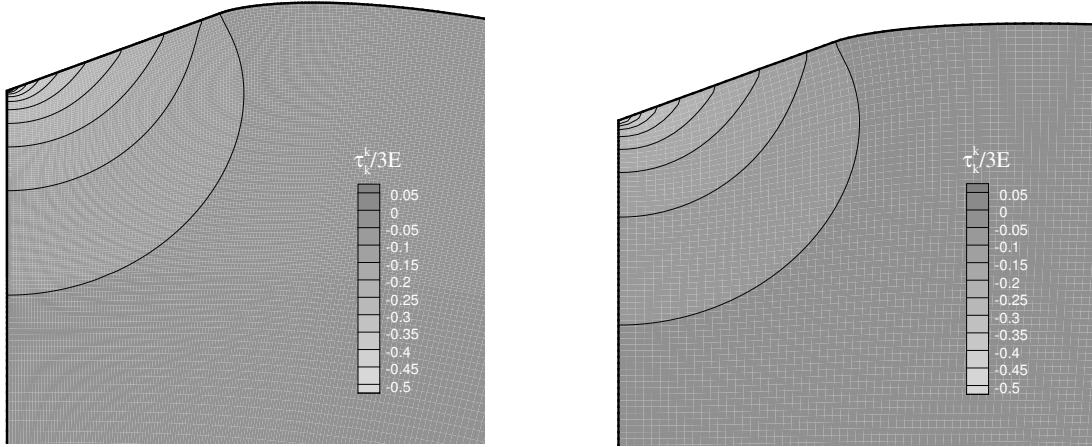
Figure 7. Contours of $\tau_k^k/3E$ at $\Delta t/t = 0.1$ in the vicinity of the indentation for the two cases shown in Figure 6: shells with $t/R_o = 0.6$ (left) and $t/R_o = 0.2$ (right).

E directly under the indenter. In fact, the stress is singular at the indenter tip and the peak value obtained there depends on the finite element discretization. In both cases, the values of τ_k^k are positive in a vicinity near $y^1 = 0$, $y^2 = R_i$ and in a vicinity near $y^1 = R_o$, $y^2 = 0$ which are indications of bending of the spherical shell. As can also be seen in the figure, the inner surface of the initially spherical shell does not quite remain spherical. The overall bending of the spherical shell gives rise to the deviation of P/Eh^2 from its value for indentation into a flat surface.

The distributions of $\tau_k^k/3E$ for these two cases in the vicinity of the indenter are shown in the bottom row in Figure 7. Near the indenter these distributions are very similar to those for indentation into a flat surface.

4. Concluding remarks

We have carried out finite deformation analyses of indentation of a rigid cone into linear elastic (actually linear hypoelastic) spherical shells. Our results indicate that if the indenter is not too flat and if the shell is not too thick, say $t/R_o \le 0.4$, there is a regime of indentation depths where the scaling of the normalized contact force is of the same form as that for a flat surface. Hence, for isotropic elastic spherical shells in this regime we can write

$$\frac{P}{Sh^2} = C \cot \beta \quad \text{or} \quad \frac{P}{Sa^2} = C \tan \beta, \tag{4-1}$$

with $S = E/(1 - \nu^2)$ and $C \approx 2$ as opposed to $\pi/2 \approx 1.57$ for indentation into a flat surface, as in (3-1) and (3-2). Our results suggest that if the actual contact area ($a = h \cot \beta$) can be measured accurately, indentation into elastic shells may be able to be used to obtain the material's elastic stiffness even though the load is not a "pure" indentation load but also includes the effects of overall shell deformation.

For a spherical shell with $t/R_o \le 0.4$, we find that C in (4-1) is only weakly dependent on the shell thickness. For a sufficiently thin spherical shell a complex non-axisymmetric deformation pattern, for example as discussed in [Vaziri and Mahadevan 2008], occurs and our axisymmetric analysis is no longer

applicable. This lower limit for the applicability of (4-1) cannot be ascertained by an axisymmetric analysis as carried out here. However, in the range where the scaling relation in (4-1) is applicable, a relatively good estimate of the elastic stiffness can be obtained without carrying out a finite element analysis. It is of interest to learn whether or not such simple scaling relations can be used to obtain an estimate of elastic stiffness for shells in more general circumstances than considered here.

Acknowledgment

References

[Barber and Ciavarella 2000] J. R. Barber and M. Ciavarella, "Contact mechanics", *Int. J. Solids Struct.* **37**:1-2 (2000), 29–43.

[Bower et al. 1993] A. F. Bower, N. A. Fleck, A. Needleman, and N. Ogbonna, "Indentation of a power law creeping solid", *Proc. R. Soc. Lond. A* **441**:1911 (1993), 97–124.

[Cheng and Cheng 1998] Y.-T. Cheng and C.-M. Cheng, "Further analysis of indentation loading curves: effects of tip rounding on mechanical property measurements", *J. Mater. Res.* **13**:4 (1998), 1059–1064.

[Doerner and Nix 1986] M. F. Doerner and W. D. Nix, "A method for interpreting the data from depth-sensing indentation instruments", *J. Mater. Res.* **1**:4 (1986), 601–609.

[Fu 2007] G. Fu, "An extension of Hertz's theory in contact mechanics", *J. Appl. Mech.* (*ASME*) **74**:2 (2007), 373–374.

[Johnson 1985] K. L. Johnson, *Contact mechanics*, Cambridge University Press, Cambridge, 1985.

[Johnson et al. 1971] K. L. Johnson, K. Kendall, and A. D. Roberts, "Surface energy and the contact of elastic solids", *Proc. R. Soc. Lond. A* **324**:1558 (1971), 301–313.

[Ma et al. 1998] D. Ma, K. Xu, and J. He, "Numerical simulation for determining the mechanical properties of thin metal films using depth-sensing indentation technique", *Thin Solid Films* **323**:1–2 (1998), 183–187.

[Oliver and Pharr 1992] W. C. Oliver and G. M. Pharr, "An improved technique for determining hardness and elastic modulus using load and displacement sensing indentation experiments", *J. Mater. Res.* **7**:6 (1992), 1564–1583.

[Oliver and Pharr 2004] W. C. Oliver and G. M. Pharr, "Measurement of hardness and elastic modulus by instrumented indentation: advances in understanding and refinements to methodology", *J. Mater. Res.* **19**:1 (2004), 3–20.

[Poon et al. 2008] B. Poon, D. Rittel, and G. Ravichandran, "An analysis of nanoindentation in linearly elastic solids", *Int. J. Solids Struct.* **45**:24 (2008), 6018–6033.

[Sneddon 1948] I. N. Sneddon, "Boussinesq's problem for a rigid cone", *Math. Proc. Cambridge Philos. Soc.* **44**:4 (1948), 492–507.

[Vaziri and Mahadevan 2008] A. Vaziri and L. Mahadevan, "Localized and extended deformations of elastic shells", *Proc. Nat. Acad. Sci. USA* **105**:23 (2008), 7913–7918.

NKEM OGBONNA: nkem42@yahoo.com
Department of Mathematics, Statistics and Computer Science, Michael Okpara University of Agriculture, Umudike, Abia State, Nigeria

ALAN NEEDLEMAN: needle@unt.edu
Department of Materials Science and Engineering, College of Engineering and Center for Advanced Scientific Computing and Modeling (CASCaM), University of North Texas, 1155 Union Circle #305310, Denton, TX 76203-50175, United States